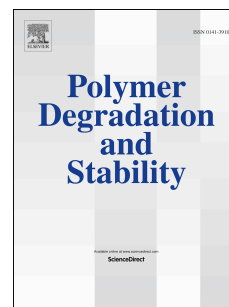


Accepted Manuscript

A comparative study of three-dimensional printing directions: The degradation and toxicological profile of a PLA/PHA blend

Jennifer Gonzalez-Ausejo, Joanna Rydz, Marta Musioł, Wanda Sikorska, Michał Sobota, Jakub Włodarczyk, Grażyna Adamus, Henryk Janeczek, Iwona Kwiecień, Anna Hercog, Brian Johnston, Habib R. Khan, Vinodh Kannappan, Keith R. Jones, Mark R. Morris, Gouzhan Jiang, Iza Radecka, Marek Kowalczyk



PII: S0141-3910(18)30125-3

DOI: [10.1016/j.polymdegradstab.2018.04.024](https://doi.org/10.1016/j.polymdegradstab.2018.04.024)

Reference: PDST 8521

To appear in: *Polymer Degradation and Stability*

Received Date: 28 February 2018

Revised Date: 11 April 2018

Accepted Date: 15 April 2018

Please cite this article as: Gonzalez-Ausejo J, Rydz J, Musioł M, Sikorska W, Sobota Michał, Włodarczyk J, Adamus Graż, Janeczek H, Kwiecień I, Hercog A, Johnston B, Khan HR, Kannappan V, Jones KR, Morris MR, Jiang G, Radecka I, Kowalczyk M, A comparative study of three-dimensional printing directions: The degradation and toxicological profile of a PLA/PHA blend, *Polymer Degradation and Stability* (2018), doi: 10.1016/j.polymdegradstab.2018.04.024.

This is a PDF file of an unedited manuscript that has been accepted for publication. As a service to our customers we are providing this early version of the manuscript. The manuscript will undergo copyediting, typesetting, and review of the resulting proof before it is published in its final form. Please note that during the production process errors may be discovered which could affect the content, and all legal disclaimers that apply to the journal pertain.

A comparative study of three-dimensional printing directions: The degradation and toxicological profile of a PLA/PHA blend

Jennifer Gonzalez-Ausejo^a, Joanna Rydz^{b,*}, Marta Musioł^b, Wanda Sikorska^b, Michał Sobota^b, Jakub Włodarczyk^b, Grażyna Adamus^b, Henryk Janeczek^b, Iwona Kwiecień^b, Anna Hercog^b, Brian Johnston^c, Habib R. Khan^c, Vinodh Kannappan^c, Keith R. Jones^c, Mark R. Morris^c, Gouzhan Jiang,^d Iza Radecka^c, Marek Kowalczyk^{b,c}

^aPolymers and Advanced Materials Group (PIMA), Universitat Jaume I, Avda. Vicent Sos Baynat s/n, 12071 Castellon, Spain

^bCentre of Polymer and Carbon Materials, Polish Academy of Sciences, 34, M. Curie-Skłodowska St, 41-819 Zabrze, Poland

^cUniversity of Wolverhampton, Faculty of Science and Engineering, Department of Biology, Chemistry and Forensic Science, Wulfruna Street, Wolverhampton, WV1 1LY, UK

^dCranfield University, School of Water, Energy and Environment, Centre for Bioenergy and Resource Management, Bedfordshire MK43 0AL, UK

Corresponding author. E-mail address: jrydz@cmpw-pan.edu.pl (J. Rydz).

ABSTRACT: The use of biobased plastics is of great importance for many applications. Blending thermoplastic polylactide (PLA) with polyhydroxyalkanoate (PHA) enables the formulation of a more mechanically powerful material and this enables tailored biodegradation properties. In this study we demonstrate the 3D printing of a PLA/PHA blend as a potential candidate for biocompatible material applications. The filament for 3D printing consisted of PHA, which contains predominantly 3-hydroxybutyrate units and a small amount of 3-hydroxyvalerate units, as revealed by multistage mass spectrometry (ESI-MSⁿ). This research

found that the properties of 3D printed species before and during abiotic degradation are dependent on printing orientation. Furthermore, the 3D printed specimens exhibited good biocompatibility with HEK293 cells, indicating real promise as biological scaffolds for tissue engineering applications.

Keywords: three-dimensional printing, layer orientation, degradation, (bio)degradable polyester, toxicity test, cell proliferation

1. Introduction

Three-dimensional (3D) printing is a rapidly-growing additive manufacturing technology that can create almost any shape three-dimensional object using digital computer-aided design (CAD). The process joins material to make an object, usually layer upon layer. Different 3D printing technologies such as fused deposition modeling (FDM), stereolithography (SL) or selective laser sintering (SLS) require variety of materials used in 3D printing. [1]

Traditional polymer materials have an adverse effect on the environment, so the use of (bio)degradable and/or biobased polymers with a minimized carbon footprint have global importance. The rapid growth of 3D printing technology enables the opportunity for the development of the (bio)degradable polymer market with (bio)degradable “inks” in the form of filaments, beads, powders, solutions and gels to produce personalized items. Thermoplastics are the only group of plastics that can be processed by extrusion and injection methods. Above a certain temperature limit thermoplastics pass in to the plasticized state, in which it is able to be shaped into large deformations. This allows for pressure forming, and also additive manufacturing. [2-6]

High biocompatibility, good mechanical properties and the low cost of polylactide and polycaprolactone (PCL) make these materials suitable for many printing technologies, however,

the widespread use of (bio)degradable polymeric “inks” hinders their lack of diversity. [1,7-9] Polyhydroxyalkanoates are the most extensively studied classes of microbial polyesters that exhibit biodegradability, good biocompatibility without any toxic effects. The blending of PHAs with other polyesters significantly improves their mechanical properties and makes materials less brittle than standard PLA. [10-13] Using PHAs in additive manufacturing opens up new possibilities for this technology [1].

Much of today’s filaments, made from petrochemical or even renewable resources, are nonbiodegradable. In addition, some commercially available biodegradable materials do not contain information about filament composition and therefore their biodegradation response is unknown. That is why it is so important to know the composition of the filaments made from biodegradable polymeric materials and predict the properties of the printed items to be able to precisely understand its properties and response to match them with specific applications [14]. Furthermore, green and sustainable polymers provide an excellent solution for many 3D printing applications. The combination of 3D printing technology and a renewable source of filaments is almost limitless in scope due to the creativity of designers, the advances in computer processing and the capacity of modern printer units [15].

The aims of this study were to determine the exact molecular structure of the PLA/PHA filament, to know the effect of processing conditions and printing orientation (horizontal and vertical processing build directions), to measure the degradation and finally to produce a toxicological profile of the filament in view of its potential application as a biocompatible scaffold.

2. Materials and methods

2.1. Materials

The materials used in this study were two commercial 3D printing filaments of 1.75 mm diameter: PLA filament (Orbi-Tech, Germany, processing temperature ≤ 205 °C) with a mass-average molar mass $M_w = 274000$ g/mol, molar-mass dispersity $M_w/M_n = 2.4$ (determined by GPC) and *D*-lactide content equal to 5.2 % estimated according to the previously described method [16] and PLA/PHA blend filament (ColorFabb, The Netherlands, processing temperature 190-210 °C), with 88 wt% of PLA (determined by TGA) and *D*-lactide content equal to 5.0 % [16]. The thermal properties of filaments (data from DSC heating run at 20 °C/min for amorphous samples after quenching) are presented in Table 1. Amorphous samples of PLA/PHA exhibited a small exothermic effect of cold crystallization at 140.4 °C ($\Delta H_{cc} = 0.35$ J/g) during heating. Both materials were used as received.

Table 1. Thermal properties of the filaments used.

Filament	T_{gPLA} [°C]	T_{mPLA} [°C]	T_{gPHA} [°C]	T_{mPHA} [°C]	ΔH_m [J/g]
PLA	61.4	-	-	-	-
PLA/PHA	59.4	153.3	1.1	173.1	11.6

T_g – glass transition temperature, T_m – melting temperature, ΔH_m – melting enthalpy

2.2. Fabrication of 3D-printed dumbbell-shaped specimens

For the purpose of these studies PLA and PLA/PHA dumbbell-shaped specimens type 1BA (specimen geometries according ISO 527 standard [17]) were prepared using a fused deposition modelling printer (FLASHFORGE Dreamer dual extrusion 3D printer). To evaluate the influence of layer orientation, specimens with two different processing build directions were printed using the methodology of 3D structures creation based on layer by layer printing. One set

of specimens was obtained with horizontal (flat, XY plane) processing build direction and with raster angle $[45^{\circ}/-45^{\circ}]$ (crisscross pattern). The second one was obtained with vertical (upright, ZX plane) processing build direction and with raster angle $[90^{\circ}]$ (transverse pattern), (Fig. 1). For specimens made in the vertical direction support material was needed that was carefully removed using a scalpel in order to not deform the specimen. Dumbbell-shaped specimens printed in the horizontal direction, had been in contact with the printer platform by 15 min; the specimen print in vertical by 40 min. The printer settings used are shown in Table 2. Acetone was used to clean the building platform of any residue after processing the specimens. A dumbbell-shaped specimen, printed in a horizontal direction with thickness of 1.80 ± 0.01 mm, had an average mass of 0.99 g for PLA and 1.01 g for PLA/PHA. The dumbbell-shaped specimen printed in vertical direction, with a thickness of 2.07 ± 0.01 mm, had an average mass of 1.34 g for PLA and 1.21 g for PLA/PHA.

Fig. 1. Two different processing build directions: parallel direction (horizontal) and perpendicular direction (vertical) used to obtain the dumbbell-shaped specimens by 3D fused deposition modelling printer.

Table 2. Printer settings for preparation dumbbell-shaped specimens.

Printer settings	Horizontal build direction	Vertical build direction
Nozzle diameter [mm]	0.4	0.4
Layer height [mm]	0.2	0.2
Perimeter shells	2	2
Top solid layers	2	2

Bottom solid layers	2	2
Infill [%]	100	100
Infill pattern	Linear	Linear
Print speed [mm/s]	50	70
Head travel speed [mm/s]	100	120
Nozzle temperature [°C]	200	195
Platform temperature [°C]	65	65

2.3. Hydrolytic degradation under laboratory condition

For the degradation experiments, according to ISO norm [18], the dumbbell-shaped specimens were incubated at 50 °C and 70 °C (± 0.5) in 30-mL screw-capped vials with an air-tight PTFE/silicone septum, containing 25 mL of demineralized water (pH = 5.6) over a period of 70 days. The specimens incubated were run in triplicate. After a predetermined degradation time, the specimens were separated from the degradation medium, washed with demineralized water and dried, first on filter paper and then under a vacuum at a temperature of 25 °C to a constant mass. After a specified period of time (1, 3, 7, 21, 42 and 70 days) surface erosion, the specimens' molar mass, molar-mass dispersity and thermal characteristics, as well as the molecular structure of the specimens, were determined. The molar mass loss was performed with triplicate measurements and calculated as described elsewhere [19,20].

2.4. Methods

2.4.1. Imaging of sample surfaces

Macroscopic changes of the surface of the samples tested were visualized using a digital camera Olympus E-410, while microscopic changes were analyzed using an optical microscope Opton-

Axioplan as described elsewhere [8]. Scanning electron microscope (SEM) studies were performed using of a Quanta 250 FEG (FEI Company, USA) high resolution environmental scanning electron microscope operated at 5 kV acceleration voltages. The samples were observed without coating under low vacuum (80 Pa) using a secondary electron detector (Large Field detector).

2.4.2. Nuclear magnetic resonance (NMR)

^1H NMR spectra were acquired at 40 °C for PLA/PHA specimens and at room temperature for PLA specimens using a Bruker-Advance spectrometer as described elsewhere [22].

2.4.3. Fourier transform infrared (FTIR) spectroscopy

Infrared spectra were recorded using a Thermo Scientific model Nicolet 6700 at room temperature in attenuated total reflection (ATR) mode with a diamond crystal. Sixty-four scans were collected in the range of 500-4000 cm^{-1} wave numbers with a spectral resolution of 4 cm^{-1} . A background scan of a clean diamond crystal was acquired before scanning the samples.

2.4.4. Gel permeation chromatography analysis (GPC)

The molar mass and molar-mass dispersity of the filaments and dumbbell-shaped bone specimens were determined using gel permeation chromatography using a Viscotek VE 1122 (Malvern, Worcestershire, UK) pump with two Mixed C PLgel styragel columns (Agilent, Santa Clara, CA, USA) in series and a Shodex SE 61 RI detector (Showa Denko, Munich, Germany) as described elsewhere [21].

2.4.5. Thermogravimetric analysis (TGA)

Thermogravimetric analysis was performed with a TGA/DSC 1 Mettler-Toledo thermal analyzer as described elsewhere [22].

2.4.6. Differential scanning calorimetry (DSC)

Thermal characteristics of the materials were obtained using the TA-DSC Q2000 apparatus (TA Instruments, Newcastle, DE, USA). The instrument was calibrated with high purity indium. The first heating run of the initial sample in which the thermal history is suppressed and the second heating run of the sample after rapid cooling were acquired from -30 °C to 220 °C at the heating rate of 20 °C/min. All of the experiments were performed under a nitrogen atmosphere with the nitrogen flow rate of 50 mL/min, using aluminum sample pans. The melting temperature (T_m) was taken as the peak temperature maximum of that melting endotherm, and the glass transition temperature (T_g) was taken as the midpoint of the heat capacity change of the amorphous sample obtained by quenching the melted samples from melt (220 °C).

2.4.7. Mechanical properties

The mechanical properties of the samples were determined by conducting tensile tests, which were carried out in accordance with norm ISO 527 in an Instron 4204 universal testing machine (England) equipped with a 1 kN cell load. The crosshead speed was 20 mm/min. The system controls and data analysis were performed using the supplied Instron IX.

2.4.8. Electrospray mass spectrometry (ESI-MS) analysis

Electrospray ionization mass spectrometry analysis of the composition of filament oligomers in a degradation medium and the solid sample after incubation was performed using a Finnigan LCQ ion trap mass spectrometer (Thermo Fisher Scientific Inc, San Jose, CA, USA) as described elsewhere [22]. The samples were dissolved in a water/methanol mixture (degradation medium) or chloroform/methanol mixture (solid sample after incubation). For multistage mass spectrometry (ESI-MS² experiments) the ions of interest were isolated monoisotopically in the ion trap and collisionally activated. Helium damping gas present in the mass analyzer acted as the collision gas.

2.5. Assessment of toxicity to human cells

2.5.1. PLA/PHA preparation for toxicity testing

The PLA/PHA dumbbell-shaped specimens were cut into 10 mm x 5 mm sections and immersed in 100 % ethanol for sterilization. Standard glass coverslips were used as controls and they were also cleaned with ethanol. Both the PLA/PHA sections and slips were allowed to dry under a vacuum for 24 hours. 50,000 HEK293 human embryonic kidney cells and 50,000 WI-38 normal human lung fibroblasts were gently pipetted onto the horizontally or vertically printed PLA/PHA sections and coverslips contained in the wells of a 24-well plate. The cells were maintained in 2 mL of RPMI medium (Lonza, Slough, UK) supplemented with 10 % fetal calf serum, 50 U/mL penicillin and 50 µg/mL streptomycin (Lonza, Slough, UK) for 24 hours at 37 °C and at 5 % CO₂.

2.5.2. SEM assessment

After up to 7 days growth, the slips and PLA/PHA specimens were removed from their wells inside a BioMAT 2 cabinet (Contained Air Solutions, Manchester, UK) using sterilized forceps. The samples were then placed into a solution of phosphate-buffered saline (PBS) with 2.5 % glutaraldehyde overnight at 4 °C for fixation. Using separate 50 % ethanol baths, the specimens were each submerged as 100 % ethanol was added (drop-wise) to bring each bath up to 90 % ethanol. The seeded PLA/PHA specimens were removed from their baths and allowed to dry in a sterile environment for 30 min. At this point the samples were covered with conductive gold *via* a sputter-coater in a vacuum chamber and analyzed at 500x to 2000x magnification using a Carl Zeiss AG – EVO[®] 50 Series (USA) SE Microscope at an accelerating voltage of 10 kV.

2.5.3. Light microscopy of human cells

PLA/PHA specimens that contained HEK293 and WI-38 cells were removed from the incubators whilst in their 24-well plates and photographed suspended in growth medium at 400x magnification using a Nikon Eclipse TS100 inverted microscope (Japan) and Nikon Digital Sight camera DS-L2 (Japan).

2.5.4. MTT assay

Cell viability was assessed by using standard MTT assay techniques. The HEK293 cells were incubated in growth media containing 5 mg/mL MTT (Sigma-Aldrich, UK) for 2 hours at 37 °C, followed by solubilization of the resulting insoluble formazan crystals with 180 µL of dimethyl sulfoxide and 20 µL of Sorensen's glycine buffer. Absorbances at 540 nm were read using a microplate reader (Multiskan™ Thermofisher scientifics, USA). Each experiment was carried out in triplicate to generate the average viability.

2.5.5. Statistical analysis of viability assay

The data pertaining to the MTT assay of HEK293 cells were recorded from horizontally and vertically printed specimens, at 540 nm absorbance of cell proliferation and replicated three times. For statistical analysis the data from days 1 to 7 were subjected to analysis of variance using statistical software (IBM SPSS 24) and the means were compared using the least significant differences (LSD) at a 5 % level of probability ($P < 0.05$).

3. Results and discussion

3.1. Verification of PLA/PHA filament composition

The study of biocompatible polymer material's behavior in different environments needs thorough understanding of their composition and molecular structure. The composition of PLA/PHA filament was determined based on ^1H NMR and ESI-MS analysis. The ^1H NMR spectrum of PLA/PHA filament showed signals corresponding to the protons of PLA

constitutional repeating units (signals 1 and 2) and signals corresponding to the protons of poly[(*R*)-3-hydroxybutyrate] (PHB) constitutional repeating units (signals 3-5), two main components of the blend (Fig. 2). The spectrum also showed low signal corresponding to the dicarboxylic acid, azelaic acid (AZA, signals 6 and 7), what also was confirmed by ESI-MS analysis (Figs 3A and 4), which more likely was added as a plasticizer or an antibacterial agent. Signals from azelaic acid were visible also in the ^1H NMR spectrum of PLA filament (data not shown). [23,24]

Fig. 2. ^1H NMR spectrum of PLA/PHA filament.

It is important to notice that, the PLA/PHA filament is not completely dissolved in chloroform. Thus, the precise quantitative analysis using NMR was not possible. Previously, the electrospray ionization multistage mass spectrometry has been successfully applied for verification of chemical structure of PHAs [25]. Therefore, the detailed molecular characterization of PLA/PHA blend was carried out by ESI-MS analysis. The ESI-MS technique enables determination of sequence distribution of monomeric units in the PHA starting from dimer up to the oligomers with M_n up to around 2000 g/mol. However, for such MS evaluation the high-molar-mass PHA copolymer should be degraded on controlled way to respective oligomers. For verification of chemical structure of PLA/PHA filament the controlled depolymerization of this blend was performed in neutral medium (demineralized water) over a period of 52 weeks at 70 °C prior to structural analysis in order to obtain soluble in chloroform low-molar-mass PHA oligomers. The ESI-MS technique provides the significant information on molecular structure of PHA component of filament after degradation in such neutral medium. The spectra can be acquired in

positive or negative mode. [26-28] Taking the advantage of various degradation rates of PLA and PHA in water the ESI-MS spectrum of PLA/PHA filament after 52 weeks of hydrolytic degradation consists in the mass range of $m/z = 60-200$ Da the negative ions of lactic acid, 3-hydroxybutyric acid and their dimers (Fig. 3A).

Moreover, the negative ion corresponding to azelaic acid was also observed at $m/z = 187$ (Fig. 3A). To verify the structural assignment of this ion the ESI-MS² experiment was performed (Fig. 4). It was revealed that both filaments (PLA and PLA/PHA) contain azelaic acid, which is added as a plasticizer or an antibacterial agent. [23,24] Furthermore, in the positive ion mode (in the mass range $m/z = 950-1300$) single-charge sodium adducts of PHA oligomers were detected (Fig. 3B).

Fig. 3. ESI-MS spectrum in the range of (A) $m/z = 60-200$ in negative-ion mode and (B) $m/z = 950-1300$ in positive-ion mode of solid sample after 52 weeks of depolymerization in neutral medium at 70 °C of PLA/PHA filament; LA – lactic acid, HB – 3-hydroxybutyrate (86 Da) and HV – 3-hydroxyvalerate (100 Da) constitutional repeating units, AZA – azelaic acid.

Fig. 4. ESI-MS² fragmentation experiment in negative-ion mode for the ion at m/z 187 assigned to azelaic acid (Fig. 3A).

In order to verify the structural assignment of the ions presented in the positive ESI-MS spectrum and to confirm the chemical structure of the PHA filament component the ESI-MS² experiment was performed. It was found that the selected ion at $m/z = 1259$ belongs to the hydroxy and carboxy end groups terminated HO-HB₁₃HV oligomer contained one 3-

hydroxyvalerate (HV) repeat unit. The ESI-MS² spectrum acquired for this ion is presented in Fig. 5 together with its theoretical fragmentation pathway.

Fig. 5. ESI-MS² fragmentation experiment in positive-ion mode for the ion of the sodium adduct at $m/z = 1259$ belongs to poly(3-hydroxybutyrate-*co*-3-hydroxyvalerate) (PHBV) series (Fig. 3B).

The random distribution of HV constitutional repeating units along the PHBV chain was confirmed in this way [25]. It is worth noting that the fragmentation of PHA positive ions takes place from both carboxy and hydroxy moieties *via* the cleavage of ester bonds along the polyester chain. These form ions consisting of 3-hydroxybutyrate (HB) and/or HV comonomer units which correspond to linear HOHB_nHV_m copolyester chains terminated by hydroxy and carboxy end groups. Therefore, the MS² experiment confirmed that the PHA component of the PLA/PHA blend consists of small amount of HV repeated units randomly distributed along the PHA chain. Thus, it was originally demonstrated that using this approach the composition of blends contained unknown PHA component may be determined with the aid of the multistage mass spectrometry. Unfortunately, this method is unable to distinguish whether the different PHA components are part of homopolymer PHBV or are part of PHA copolymers (PHB and PHBV). [29]

3.2. *The effect of printing directions on the properties of 3D-printed dumbbell-shaped specimens*

Building directions determine not only the quality of the specimen, manufacturing time and volume of the material used but also properties of obtained specimens [30,31]. The effect of building directions on the properties of 3D-printed dumbbell-shaped specimens obtained from

PLA and PLA/PHA commercial filaments were investigated using SEM and DSC techniques as well as the tensile test.

Three-dimensional printing in horizontal or vertical processing build directions showed a significant influence on structure and morphology of the specimens (Fig. 6). When specimens were printed in horizontal direction upper and underside layers had surfaces with different characteristic. It is related with the fact that one layer is in contact with the 3D-printer platform. Indeed, in the case of fused deposition modelling, the technique of rapid prototyping, the heated thermoplastic polymer filament is extruded from a tip that moves in the XY plane. The controlled extrusion head deposits polymeric material onto the build printer platform to form at first, the underside layer. The printer platform is kept at not too high temperature (65 °C, see Table 2) so that the thermoplastic material hardens quickly. However, polymeric material is permanently maintained at a constant temperature during printing which can affect properties of the material. The extrusion head deposits layer by layer in the Z-axis. The process is continued to produce the desired specimen. [32-35] The upper layer is the furthest from the platform (Fig. 6, UH and BH layers).

Vertical direction does not affect the structure of the surfaces of the PLA or PLA/PHA specimens because the contact with the printer platform was only at the small area in the base of the dumbbell-shaped specimen. No difference was also observed between both polymer materials, while printed in the vertical direction (Fig. 6, V).

Fig. 6. Selected SEM micrographs of upper (UH) and underside (BH) layers of PLA dumbbell-shaped specimens surface obtained by 3D printing in horizontal (H) and vertical (V) directions.

In order to evaluate the changes in the thermal properties of the tested samples as a consequence of the thermal history during the processing by 3D printing, DSC analysis was conducted (Table 3). The cold crystallization temperature (T_{cc}), the melting temperature and the enthalpy values (ΔH_{cc} and ΔH_m) were measured from the first calorimetric trace (first heating run) for the plain sample and from the second heating run for the amorphous samples obtained by rapid cooling from the melt. The glass transition temperature were taken for the amorphous samples.

Table 3. Calorimetric parameters of PLA and PLA/PHA filament and dumbbell-shaped specimens obtained by 3D printing in horizontal (H) and vertical (V) directions (I-heating run and II-heating run after rapid cooling, 20 °C/min).

	PLA filament	PLA-H	PLA-V dumbbell from platform side	PLA-V dumbbell from other side	PLA/PH A filament	PLA/PH A-H	PLA/PH A-V dumbbell from platform side	PLA/PH A-V dumbbell from other side
I-heating run								
T_m [°C]	-	150.7	150.0	150.6	153.3/173 .1	153.5/172 .2	153.7/171 .9	154.4/173 .4
ΔH_m [J/g]	-	0.98	1.82	1.85	11.64	16.16	13.88	10.04
T_{cc} [°C]	-	118.0	131.6	113.8	125.7	116.5	123.4	128.5
ΔH_{cc} [J/g]	-	-0.93	-1.80	-1.84	-11.50	-16.70	-13.62	-9.97
II-heating run								
T_g [°C]	61.4	62.2	61.8	61.7	1.1/59.4	1.9/62.8	2.2/60.6	1.6/60.3
Δcp	0.48	0.50	0.51	0.50	0.03/0.46	0.04/0.49	0.06/0.49	0.02/0.49

[J/g°C]								
T_m [°C]	-	-	-	-	151.4/173	172.4	153.6/175	152.1/173
					.1		.3	.8
ΔH_m [J/g]	-	-	-	-	0.16/0.19	0.24	0.51	0.61
T_{cc} [°C]	-	-	-	-	140.4	136.8	140.9	142.2
ΔH_{cc} [J/g]	-	-	-	-	-0.35	-0.23	-0.47	-0.60

T_g – glass transition temperature, Δcp – the increment of heat capacity at the glass transition, T_m – melting temperature, ΔH_m – melting enthalpy, T_{cc} – maximum of the exothermic peak of the cold crystallization temperature, ΔH_{cc} – cold crystallization enthalpy

During 3D printing, tensile forces act upon the filament, which result in a tension induced crystallization and orientation of the layers in dumbbell-shaped specimens. [36,37] During printing dumbbell-shaped specimens, printed in horizontal direction, had longer contact with the printer platform and are permanently maintained at a constant temperature which affects the thermal properties of the material. In the case of dumbbell-shaped specimens printed in the vertical direction, this effect is less significant because the contact with the printer platform was only at the small area in the base of the dumbbell-shaped specimen. The upper part of the dumbbell, further from the platform, had no contact with it, and thus for the vertical specimens only the dumbbells from the platform side was affected. Therefore, both ends were investigated. The DSC results of the PLA filament show only a glass transition temperature, $T_g = 61.4$ °C (Table 3) suggesting that the filament is amorphous. The PLA dumbbell-shaped specimens, in the first heating run, exhibit a melting process with a maximum temperature around 150 °C for all specimens. The melting enthalpies for both sides of the specimens printed in vertical direction were the same and higher than for specimens printed in the horizontal direction. The processing

(3D printing), therefore causes an increase in the crystalline phase of the specimen compared to the starting filament. After 3D printing a slight increase in T_g was also observed as a result of the increase in crystalline domains, which could also increase the stiffness [38].

Regarding the DSC results of the PLA/PHA filament, the first heating run showed the crystallization phenomenon at $T_{cc} = 125.7$ °C (associated with the presence of PHA component) and two melting temperatures at $T_{m1} = 153.3$ °C and $T_{m2} = 173.1$ °C. The first is related to the melting temperature of PLA crystallites and the second corresponds to the melting temperature of PHA component crystallites. The increase in melting enthalpy in relation to the PLA filament was also observed. The presence of the PHA component (as the nucleation agent) initiates the growth of the crystalline phase of the filament by induction/nucleation [39]. Two glass transition temperatures were observed for the PLA/PHA filament and both specimens indicating that the PLA/PHA blend is immiscible and exhibits phase separation in the melt [40,41]. Both PLA/PHA dumbbell-shaped specimens, in the first heating run, also exhibit melting processes related to the melting temperatures of both the main components of crystallites, PLA and PHA. The melting enthalpy for specimens printed in the horizontal direction has higher value indicating an increase in the crystalline phase during processing in a horizontal build direction. This is due to the dumbbell-shaped specimen printed in the horizontal direction had longer contact with the printer platform. The melting enthalpy for a specimens printed in the vertical direction for dumbbells from platform side, also increased slightly compare to the other side and to PLA/PHA filament. After 3D printing an increase in T_g of both components were also observed.

At a cooling rate of 10 °C/min (II-run), the PLA/PHA dumbbell-shaped specimen obtained by 3D printing in horizontal direction does not crystallize because the crystallization rate is very slow. However, at cooling rate of 2 °C/min one exotherm at crystallization temperature $T_c =$

111.2 °C (with crystallization enthalpy, $\Delta H_c = 11.39$ J/g) is observed, and at cooling rate of 1 °C/min the two exotherms at $T_c = 100.8$ °C and $T_c = 123.6$ °C (with $\Delta H_c = 18.25$ J/g) are observed. A slower heating rate allows nucleation and crystal growth in the sample. Further extension of the crystallization time allows to obtain a higher degree of crystallinity (this corresponds to an increase in the enthalpy of crystallization from 11.39 J/g to 18.25 J/g). The likely explanation of the multimodal DSC thermogram through two overlapping phenomena: as the result of the crystallization of (i) different populations of macromolecules with different molar mass or (ii) the populations of the two components of the blend (PLA and PHA).

The mechanical properties of dumbbell-shaped specimens were determined performing tensile tests. Fig. 7 shows the Young's modulus (E), tensile strength (σ_y), and elongation at break (ϵ_R) of PLA and PLA/PHA dumbbell-shaped specimens obtained by 3D printing as a function of the processing build direction.

Fig. 7. Young's modulus, tensile strength, and elongation at break of PLA and PLA/PHA dumbbell-shaped specimens obtained by 3D printing in horizontal (H) and vertical (V) directions.

The Young's modulus, tensile strength and elongation at break showed greater values for dumbbell-shaped specimens printed in the vertical direction which is associated with orientation and defects of the filament layers as well as thickness of the specimens. The Young's modulus is an indication of the relative stiffness of material. The same material this can vary greatly depending on the orientation of the filament layers in the material matrix. Transverse orientation increases the Young's modulus for vertical processing build direction [42]. The tensile strength

also depends on the filament layers orientation with respect to the stress direction, but also depends on the density of the material matrix and thickness of the specimens. Longitudinal tensile strength should be higher than that of the transverse direction because cohesion between the two printed layers is weaker. The material should be stronger along the direction of the orientation of the filament and weakest in a direction perpendicular to the filament. Also a strong material should be relatively denser. [43,44] The reason for the lower tensile strength in the case of specimens printed in the horizontal direction (the force applied longitudinally to the filament) may be that the polymer matrix had defects (caused by arrangement of the filament) as hollow spaces (see Fig. 6) and specimens were thinner which principally reduces the tensile strength of the material. In particular, the PLA specimens, which were processed in a vertical build direction, had a slight increase in Young's modulus and elongation at break of about 10 % and 18 %, respectively in relation to the values for dumbbell-shaped specimen printed in the horizontal direction. The effect of the direction in the tensile strength of PLA dumbbell-shaped specimens had even an increase about of 55 % compared to the dumbbell-shaped specimen printed in horizontal direction. The processing build direction also causes some differences in the mechanical properties of PLA/PHA dumbbell-shaped specimens. The increment in Young's modulus and tensile strength was about 8 % and 20 %, respectively for vertical specimens. These values were lower than for PLA specimens. Nevertheless, the vertical direction resulted in a marked increase in the elongation at break for PLA/PHA specimen ($\epsilon_R = 4.5$ %) compared with PLA specimen ($\epsilon_R = 2.9$ %). This may explain the higher thickness of the specimen as well as the presence of a small amount of PHA in the blend that acts on this induction/nucleation as can be seen from the DSC results (see Table 3). Nucleation improves the mechanical properties of the polymer material and enhances its strength and stiffness. Nucleate causes a uniform dispersion of

small crystallites in the polymer, which increases the Young's modulus, impact strength, tensile strength, impact resistance, an increase in the heat deflection temperature and the bending module. [45-47]

From the macrographic images of the studied samples after mechanical tests (Fig. 8) morphological differences can be observed in the fracture.

Fig. 8. Macro- and micrographic images of the PLA and PLA/PHA dumbbell-shaped specimens obtained by 3D printing in horizontal (H) and vertical (V) directions after tensile test.

Specimens processed in the horizontal build direction showed a very irregular breaking area. This fact can be explained by the filament arrangement according to the algorithm used to process the specimens. When the tensile test was performed, the force was applied in the longitudinal direction to the specimen, in which the filament was deposited by changing the angle with respect to this direction with raster orientation $[45^{\circ}/-45^{\circ}]$. While all the layers that composed the vertical specimens were placed at 90° with respect the longitudinal direction (direction of force application on tensile tests). Therefore, the adhesion between layers is different. As can be seen from Fig. 9, the fracture for the vertical specimen presents a sharp shape edge and smooth surface, and the fracture for horizontal specimen exhibit at irregular surface.

Vertical specimens with the layers oriented perpendicular to the load direction had improved mechanical properties (Young's modulus, tensile strength and elongation were higher, indicating that the material was stiffer, stronger and more flexible) more than horizontal specimens with the

layers oriented parallel to the load direction. This is possibly due to more homogenous and dense material matrix as well as crystallization induced by deformation.

Orientation ensures more crystallization while the chains and crystalline structure align in the direction of stretching. Orientation improves the tensile and impact strengths, stiffness, clarity and durability, as well as leads to higher values of the elastic modulus of the polymer materials.

On the other hand, orientation may cause detrimental effects on elongation. [48-50]

3.3. Toxicity analysis

Biodegradable polymers as well as their additives should be environmentally friendly, nontoxic and biocompatible depending on the application. For these reasons toxicity studies were conducted to assess the potential hazards of the PLA/PHA blend. A number of cell cultures are used to measure cell toxicity, basic cell functions and specialized cells are used to estimate parameters. In general toxicity *in vitro* studies, a diploid human fibroblast line such as WI-38 is used as it is well-characterized and easy to culture. A cell line such as HEK293 can also be used because they are also easy to maintain and have quicker and more reliable rates of proliferation [51]. The viability of these cells was assessed by microscopic observation and the metabolic activity of a population of HEK293 was measured by MTT assay to investigate cell proliferation. The morphology of normal WI-38 human lung fibroblast cells and HEK293 human embryonic kidney cells was observed after 48 hours growth to confirm the phenotype of the cells before *in vitro* studies commenced. The WI-38 cells exhibited irregular morphology and marginal ruffling, as observed in previous studies, while HEK293 cells clearly showed the characteristics of immature neurons, consistent with their origins [51] (Fig. 9).

Fig. 9. Selected photomicrographs (400x magnification): (A) WI-38 fibroblasts cells with expected irregular morphology, (B) HEK293 cells showing neuron-like shapes.

Due to the crisscross pattern used to produce the horizontal specimens (created as the filament was deposited at a changing angle with respect to the longitudinal direction) these specimens did not give clear, comparative images for WI-38 and HEK293 cell growth. In addition, the thinner and irregular cellular composition of WI-38 cells also made light microscopy an impractical method of demonstrating fibroblast growth effectively. Instead only the HEK293 cells on vertically printed specimens were used for the light-microscope analysis and SEM analysis to show biocompatibility on horizontal (and vertical specimens for comparison) PLA/PHA blend specimens for WI-38 cell growth.

Both types of cells were able to grow on the PLA/PHA blend specimens. Fig. 10 shows the horizontally and vertically printed specimens at 500x magnification after 2 and 7 days incubation (at 37 °C) when seeded with WI-38 and HEK293 cells. The cells were able to grow on the surface of the PLA/PHA blend specimens and within the spaces of the lattice created during the 3D printing process. The appearances of the cells were consistent with healthy cultures, indicating that the blend is nontoxic.

Fig. 10. Selected SEM micrographs of cells at 500x magnification after 2 days and 7 days incubation on horizontally (H) and vertically (V) printed PLA/PHA blend specimens. Images sequentially illustrate control test (specimen without cells), specimens with WI-38 cells and specimens with HEK293 cells.

The HEK293 cell images (Fig. 10) appear more defined on the horizontally printed specimens due to flatness and therefore having better contact and conductance when mounted on the SEM stubs as compared to the slightly convex-shaped vertically printed specimens. As HEK293 cells were more visible than WI-38 for photomicroscopy and their growth rate was more consistent, HEK293 were selected for further analysis on the both vertically printed and horizontally printed specimens (Figs 11).

Fig. 11. Selected photomicrographs (40x and 400x magnification) of HEK293 cell growth after 2 days and 7 days incubation on horizontally (H) and (V) vertically printed PLA/PHA blend specimens.

The MTT assay with HEK293 on horizontally and vertically printed specimens was used to add numerical value to the qualitative microscopic observations. Fig. 12 shows the horizontally printed specimen tended to produce more growth from day 4 onwards. The results also show a highly significant interaction ($P < 0.01$) between the horizontal and the vertical specimens and duration. The absorbance recorded after 7 days was much higher in horizontal position ($A = 3.79$) when compared with the vertical orientation ($A = 2.42$). This shows further indication of more growth on the horizontal printed specimen.

Fig. 12. MTT assay of HEK293 cells on horizontally and vertically printed specimens, where absorbencies (at 540 nm) in arbitrary units are equivalent to formazan absorbance as a measure of cell proliferation. The vertical error bars represent standard error based on three replications.

The spaces in the crisscross pattern of the horizontally printed specimen may provide zones where cells can attach and proliferate more successfully than the convex, vertical prints as this would account for the observed trend. These data also show that as long as the media is replaced regularly, both of the cell lines used could continue to grow on PLA/PHA blends for 7 days with no observed toxicity.

3.4. Hydrolytic degradation of PLA and PLA/PHA dumbbell-shaped specimens

The hydrolytic degradation of PLA and PLA/PHA dumbbell-shaped specimens at 50 °C and 70 °C was performed under laboratory conditions over a period of 70 days. The progress of material hydrolysis was estimated by material examination and failure analysis (macro- and microscopic observations of the specimens' surfaces), as well as molecular structure and thermal properties changes during the performed experiments.

Macroscopic visual evaluation of the PLA and PLA/PHA dumbbell-shaped specimens during the degradation process showed erosion through the breaking of the specimens, which began at day 3 of incubation for all specimens degraded at 70 °C and at day 42 of incubation for all specimens degraded at 50 °C. Disintegration of the specimens began at day 7 of incubation for all specimens degraded at 70 °C. Over time, fragments become smaller. Dumbbell-shaped specimen printed in the horizontal direction resulted in finer fragments for degradation at 70 °C. The effect of build directions on the degradation of 3D-printed dumbbell-shaped specimens is more visible for degradation at 50 °C. PLA and PLA/PHA dumbbell-shaped specimens printed in horizontal direction after 70 days of degradation showed erosion through the breaking of the specimens, while those printed in the vertical direction were disintegrating. Dumbbell-shaped specimen printed in the horizontal direction resulted in an extension of the disintegration time at 50 °C (Fig. 13).

Fig. 13. Macrographic images of the PLA and PLA/PHA dumbbell-shaped specimens obtained by 3D printing in horizontal (H) and vertical (V) directions before and during hydrolytic degradation test at 50 °C and 70 °C.

PLA dumbbell-shaped specimens printed in the horizontal direction exhibited considerable deformation during degradation as a consequence of the algorithm used to process the specimens (crisscross pattern). PLA dumbbell-shaped specimens printed in the vertical direction with layers located at 90° with respect to the longitudinal direction exhibited slightly less deformation during degradation. It is known that the main disadvantage of PLA is its deformation at relatively low temperatures especially above the glass transition temperature [52]. The PHA component of the PLA/PHA dumbbell-shaped specimens leads to a significant reduction in deformation during degradation. The PLA dumbbell-shaped specimens were more transparent before the hydrolytic degradation than the PLA/PHA dumbbell-shaped specimens (yellowish in color) as a consequence of the PHA content in the blend), however a decrease in transparency of which both specimens studied, were observed after 1 day of degradation at 50 °C and 70 °C, what is common for PLA-based material as an effect of an increase in the degree of crystallinity. [19,53]

Microscopic evaluation of the specimen surface, during the degradation process indicated erosion due to water absorption as roughness of the surface of dumbbell-shaped specimens in both aging temperatures, at 50 °C and 70 °C (Figs 14 and 15). However, in the case of the degraded material above T_g of PLA, this process at the same molar mass loss (over 90 % in 7 days at 70 °C and 70 days at 50 °C), leads to larger surface damage such as cracking (Fig. 14).

Fig. 14. Selected SEM micrographs of fractures of PLA and PLA/PHA dumbbell-shaped specimens obtained by 3D printing in horizontal (H) and vertical (V) directions before degradation (0) and at the equal molar mass loss after 70 days of hydrolytic degradation test at 50 °C and after 7 days of hydrolytic degradation test at 70 °C.

Fig. 15. Selected photomicrographs (120x) of underside and upper layers of PLA and PLA/PHA dumbbell-shaped specimens surface obtained by 3D printing in horizontal (H) and vertical (V) directions before and after 42 days under hydrolytic degradation test at 50 °C and 70 °C.

The structural analysis of the dumbbell-shaped specimens after the specified degradation times was investigated by means FTIR analysis. No significant changes were observed in the structure of the PLA specimens after degradation (data not shown). During degradation, the broadening of the signal of the carbonyl group stretching frequency (around 1760 cm^{-1}) was observed due to an increase in crystallinity. This is a consequence of faster degradation of the amorphous phase, as well as in the number of carboxy end groups in the polymer chain during hydrolytic degradation. This was also observed for PLA component of the PLA/PHA dumbbell-shaped specimens (Fig. 16). Growth of the crystalline phase during degradation resulted in the shift towards higher wavenumbers; however, the carbonyl group stretching vibration of short PLA chains shift towards lower wavenumbers. [54,55] After 7 days of hydrolytic degradation of the PLA/PHA dumbbell-shaped specimens at 50 °C and 70 °C, the carbonyl group stretching frequency, associated with the crystalline (around 1723 cm^{-1}) and amorphous (around 1740 cm^{-1}) phases of the PHA appeared, due to the slower degradation rate of the PHA component of the PLA/PHA blend. [56] For PLA/PHA specimens incubated at 50 °C, the intensity of this signals was lower

due to a slow degradation rate (Fig. 16). During degradation of PLA/PHA dumbbell-shaped specimens, the signal of the carbonyl group the stretching vibration of PLA shift towards lower wavenumbers overlapped with the signal of the carbonyl group stretching vibration of the amorphous phases of the PHA component.

Fig. 16. Overlay of selected FTIR spectra of PLA/PHA dumbbell-shaped specimens obtained by 3D printing in horizontal (H) and vertical (V) directions before (0) and after 7, 21, 42 days of degradation at 50 °C and 70 °C.

The changes in the thermal properties during hydrolytic degradation of PLA and PLA/PHA dumbbell-shaped specimens printed in horizontal and vertical directions were examined using TG analysis. TG thermograms showed that the averages of the total mass loss at 400 °C for all of the investigated specimens were on the order of 100 % (Fig. 17).

Fig. 17. Overlay of selected TG and first-derivative TG thermograms (DTG) of PLA and PLA/PHA dumbbell-shaped specimens obtained by 3D printing in horizontal (solid line on the graph) and vertical (dotted line on the chart) directions before (0) and after 7, 21, 42 days of degradation at 70 °C.

During degradation at 50 °C, no significant changes were observed in the thermal stability of PLA in PLA and PLA/PHA dumbbell-shaped specimens. However, in the presence of the PHA component the increase of thermal stability was noticed. The first step of mass loss, related to thermal degradation of the PHA component, with $T_{max} = 300 \pm 1$ °C before degradation

experiment, slightly shifts toward higher temperature ($T_{max} = 308 \pm 1$ °C after 70 days of incubation for both printing directions). A shift towards a higher T_{max} value indicates an increase in polymer stability in particular of the PHA component, as a result of self-compatibilization (improve components miscibility) and the plasticizing effect of the oligomeric products generated during degradation of the PLA/PHA blend. [57,58]

During degradation at 70 °C of PLA/PHA dumbbell-shaped specimens printed in both directions, the first step of mass loss, related to thermal degradation of PHA, also shifts toward higher temperatures with $T_{max} = 310$ °C after 21 days of incubation and then decrease. The second one, related to thermal degradation of PLA (with $T_{max} = 365 \pm 1$ °C before degradation) shifts toward lower temperatures as a consequence of PLA degradation. For the PLA dumbbell-shaped specimens shifts toward lower temperatures together with broadening of the step of mass loss were found. The decomposition of dumbbell-shaped specimens after degradation confirms the degradation profile, which can lead to the formation of dual populations of PLA crystallites. [41]

4. Conclusions

Analysis of commercial PLA/PHA filament revealed that the PHA component in the blend contains mostly HB and a small amount of HV units. The processing conditions, in particular the contact time with the printer platform during printing the specimen and the filament arrangement according to the algorithm used to process the specimens, leads to different thermal and mechanical properties of material as well as the degradation profile of investigated PLA and PLA/PHA specimens'. It was originally observed that vertical specimens have improved mechanical properties compared to horizontal specimens, possibly due to more homogenous and dense material matrix as well as crystallization induced by deformation. Thermal stability of the degraded specimens has been improved as a result of self-compatibilization that improve

components miscibility and giving plasticizing effect of the oligomeric products generated during degradation of the PLA/PHA blend. Effect of build directions on the degradation of 3D-printed dumbbell-shaped specimens is more visible for degradation at 50 °C. Dumbbell-shaped specimens printed in the horizontal direction results in an extension of the disintegration time. The 3D printed materials has no toxicity to cell growth and exhibit good biocompatibility with HEK293 cells. Based on the results presented, the 3D printed material exhibits favorable mechanical properties, thermal stabilities, and cell viability, which allows PLA/PHA blend to be widely applied in many fields, especially as a good potential candidate for tissue engineering applications. However, the three-dimensional printing directions should be taken into account in the further studies.

Acknowledgments

The work was supported by Pla de Promoció de la Investigació de la Universitat Jaume I (PREDOC/2012/32 and E-2016-32), the National Scholarship Programme of the Slovak Republic for the support of mobility of students, PhD students, university teachers, researchers and artists. Partial financial support from: the Research Investment Fund, University of Wolverhampton (Wolverhampton, U.K.); the European Regional Development Fund Project EnTRESS No 01R16P00718 and the PELARGODONT Project UM0-2016/22/Z/STS/00692 financed under the M-ERA.NET 2 Programme of Horizon 2020 are gratefully acknowledged.

Author Contributions

The manuscript was written through contributions of all authors. J. Rydz contributed 50 %, J. Gonzalez-Ausejo contributed 10 %, while other authors within 40 % contributed equally to this work. All authors have given approval to the final version of the manuscript.

Notes

The authors declare no competing financial interest.

References

- [1] Włodarczyk J, Sikorska W, Rydz J, Johnston B, Jiang G, Radecka I, Kowalczyk M. Chapter 6: 3D processing of PHA containing (bio)degradable materials. In: Koller M, editor. Current advances in biopolymer processing & characterization, Biomaterials – properties, production and devices series. New York: Nova Science Publishers, 2017. pp. 121-168.
- [2] Stansbury JW, Idacavage MJ. 3D printing with polymers: challenges among expanding options and opportunities. *Dent Mater* 2016;32:54-64. doi:10.1016/j.dental.2015.09.018
- [3] Masood SH. Intelligent rapid prototyping with fused deposition modeling. *Rapid Prototyp J* 1996;2:24-33. doi:10.1108/13552549610109054
- [4] Cooke MN, Fisher JP, Dean D, Rimnac C, Mikos AG. Use of stereolithography to manufacture critical-sized 3D biodegradable scaffolds for bone in growth. *J Biomed Mater Res Part B Appl Biomater* 2003;64B(2):65-69. doi:10.1002/jbm.b.10485.
- [5] Tumbleston JR, Shirvanyants D, Ermoshkin N, Januszewicz R, Johnson AR, Kelly D, Chen K, Pinschmidt R, Rolland JP, Ermoshkin A, Samulski ET, DeSimone JM. Continuous liquid interface production of 3D objects. *Science* 2015;347:1349-1352. doi:10.1126/science.aaa2397.
- [6] Chia HN, Wu BM. Recent advances in 3D printing of biomaterials. *J Biol Eng* 2015;9(4):2-14. doi:10.1186/s13036-015-0001-4
- [7] Ford SLN. Additive Manufacturing Technology: Potential Implications for U.S. Manufacturing Competitiveness. *J Int Comm Econ* 2014;35 pages.
- [8] Guvendiren M, Molde J, Soares RMD, Kohn J. Designing biomaterials for 3D printing. *ACS Biomater Sci Eng* 2016;2:1679-1693. doi:10.1021/acsbiomaterials.6b00121.

- [9] Imre B, Pukánszky B. Compatibilization in bio-based and biodegradable polymer blends. *Eur Polym J* 2013;49(6):1215-1233. doi:10.1016/j.eurpolymj.2013.01.019.
- [10] Muhammadi, Shabina, Afzal M, Hameed S. Bacterial polyhydroxyalkanoates-eco-friendly next generation plastic: Production, biocompatibility, biodegradation, physical properties and applications. *Green Chem Lett Rev* 2015;8(3-4):56-77. doi:10.1080/17518253.2015.1109715.
- [11] Koller M, Maršálek L, de Sousa Dias MM, Braunegg G. Producing microbial polyhydroxyalkanoate (PHA) biopolyesters in a sustainable manner. *N Biotechnol* 2017;37:24-38. doi:10.1016/j.nbt.2016.05.001.
- [12] Kourmentza C, Plácido J, Venetsaneas N, Burniol-Figols A, Varrone C, Gavala HN, Reis MAM. Recent Advances and Challenges towards Sustainable Polyhydroxyalkanoate (PHA) Production. *Bioengineering* 2017;4(2):55. doi:10.3390/bioengineering4020055.
- [13] Jost V, Kopitzky R. Blending of polyhydroxybutyrate-co-valerate with polylactic acid for packaging applications-reflections on miscibility and effects on the mechanical and barrier properties. *Chem Biochem Eng Q* 2015;29(2):221-246. doi:10.15255/CABEQ.2014.2257.
- [14] Höglund A, Odelius K, Albertsson, A.-C. Crucial differences in the hydrolytic degradation between industrial polylactide and laboratory-scale poly(L-lactide). *ACS Appl Mater Interfaces* 2012;4:2788-2793. doi:10.1021/am300438k.
- [15] Zhu Y, Romain C, Williams CK. Sustainable polymers from renewable resources. *Nature* 2016;540:354-362. doi:10.1038/nature21001.
- [16] Farrington DW, Lunt J, Davies S, Blackburn RS. Poly(lactic acid) fibres. In: Blackburn RS, editor. *Biodegradable and sustainable fibres*. Cambridge: Woodhead Publishing Limited, 2005. pp. 191-220.

- [17] ISO 527–2:2012 Plastics – Determination of tensile properties – Part 2: Test conditions for moulding and extrusion plastics.
- [18] ISO 15814:1999. Implants for surgery – Copolymers and blends based on polylactide – In vitro degradation testing.
- [19] Rydz J, Adamus G, Wolna-Stypka K, Marcinkowski A, Misiurska-Marczak M, Kowalczyk MM. Degradation of polylactide in paraffin and selected protic media. *Polym Degrad Stab* 2013;98:316-324. doi:10.1016/j.polymdegradstab.2012.09.010.
- [20] Sikorska W, Richert J, Rydz J, Musioł M, Adamus G, Janeczek H, Kowalczyk M. Degradability studies of poly(L-lactide) after multi-reprocessing experiments in extruder. *Polym Degrad Stab* 2012;97:1891-1897. doi:10.1016/j.polymdegradstab.2012.03.049.
- [21] Sikorska W, Rydz J, Wolna-Stypka K, Musioł M, Adamus G, Kwiecień I, Janeczek H, Duale K, Kowalczyk M. Forensic engineering of advanced polymeric materials – Part V: Prediction studies of aliphatic–aromatic copolyester and polylactide commercial blends in view of potential applications as compostable cosmetic packages. *Polymers* 2017;9(257):15 pages. doi:10.3390/polym9070257.
- [22] Rydz J, Wolna-Stypka K, Adamus G, Janeczek H, Musioł M, Sobota M, Marcinkowski A, Krzan A, Kowalczyk M. Forensic engineering of advanced polymeric materials. Part 1 – Degradation studies of polylactide blends with atactic poly[(R,S)-3-hydroxybutyrate] in paraffin. *Chem Biochem Eng Q* 2015;29(2):247-259. doi:10.15255/CABEQ.2014.2258.
- [23] Asrar J, Shah DT, Tran M. Hydroxy-terminated polyhydroxyalkanoates. U.S. Patent 6248862 B1, August 17, 2000.
- [24] Corma A, Iborra S, Velty A. Chemical Routes for the Transformation of Biomass into Chemicals *Chem Rev* 2007;107:2411-2502. doi:10.1021/cr050989d.

- [25] Adamus G, Sikorska W, Montaudo M, Scandola M, Kowalczyk M. Sequence distribution and fragmentation studies of bacterial copolymer - characterisation of PHBV macroinitiator by Electrospray Ion-Trap Multistep Mass Spectrometry. *Macromolecules* 2000;33:5797-5802. doi:10.1021/ma000005g.
- [26] Kwiecień I, Adamus G, Kowalczyk M. Electrospray ionisation mass spectrometry molecular-level structural characterisation of novel phenoxycarboxylic acid-oligo(3-hydroxybutyrate) conjugates with potential agricultural applications. *Rapid Commun Mass Spectrom* 2012;26:2673-2682. doi:10.1002/rcm.6391.
- [27] Kwiecień I, Adamus G, Bartkowiak A, Kowalczyk M. Synthesis and structural characterization at the molecular level of oligo(3-hydroxybutyrate) conjugates with antimicrobial agents designed for food packaging materials. *Des Monomers Polym* 2014;17(4):311-321. doi:10.1080/15685551.2013.840505.
- [28] Nielsen KF, Smedsgaard J, Larsen TO, Lund F, Thrane U, Frisvad JC. Chemical identification of fungi. Metabolite profiling and metabolomics. In: Arora DK, editor. Chapter 2: Fungal biotechnology in agricultural, food, and environmental applications. New York: CRC Press, 2004. pp. 19-35.
- [29] Tan GYA, Chen CL, Li L, Ge L, Wang L, Razaad IMN, Li Y, Zhao L, Mo Y, Wang JY. Start a research on biopolymer polyhydroxyalkanoate (PHA): A review. *Polymers* 2014;6:706-754. doi:10.3390/polym6030706.
- [30] Alharbi N, Osman R, Wismeijer D. Effects of build direction on the mechanical properties of 3D-printed complete coverage interim dental restorations. *J Prosthet Dent* 2016;115(6):760-7. doi:10.1016/j.prosdent.2015.12.002.

- [31] Chen Q, Mangadlao JD, Wallat J, De Leon A, Pokorski JK, Advincula RC. 3D printing biocompatible polyurethane/poly(lactic acid)/graphene, oxide nanocomposites: anisotropic properties. *ACS Appl Mater Interfaces* 2017;9:4015-4023. doi:10.1021/acsami.6b11793.
- [32] Daneshmand S, Aghanajafi C. Description and modeling of the additive manufacturing technology for aerodynamic coefficients measurement. *J Mech Eng* 2012;58(2):125-133. doi:10.5545/sv-jme.2010.238.
- [33] Daneshmand S, Aghanajafi C, Nadooshan AA. The effect of chromium coating in RP technology for airfoil manufacturing. *Sadhana* 2010;35(5):569-584. doi:10.1007/s12046-010-0036-7.
- [34] Hutmacher DW. Scaffolds in tissue engineering bone and cartilage. In: Williams D, editor. *The Biomaterials: Silver Jubilee Compendium*, 1st edn, Elsevier: Oxford, 2006. pp. 175-189. doi:10.1016/S0142-9612(00)00121-6.
- [35] Christiyan KGJ, Chandrasekhar U, Venkateswarlu K. A study on the influence of process parameters on the Mechanical Properties of 3D printed ABS composite. *IOP Conf Ser: Mater Sci Eng* 2016;114(012109). doi:10.1088/1757-899X/114/1/012109.
- [36] Anderson KA, Randall JR, Kolstad JJ. Polylactide molding compositions and molding process. *Nature Word Patent* WO 2011085058 A1, January 6, 2011.
- [37] Schafer K. Method for melt spinning filament yarns. *US Patent* US 6824717 B2, March 6, 2002.
- [38] Sichina WJ. Measurement of T_g by DSC, PETech-09. In: *Thermal Analysis Application note*. Norwalk: PerkinElmer, Inc, 2000.

- [39] Di Lorenzo ML, Sajkiewicz P, Gradys A, La Pietra P. Optimization of melting conditions for the analysis of crystallization kinetics of poly(3-hydroxybutyrate). *e-Polymers* 2009;27:12 pages.
- [40] Kikkawa Y, Suzuki T, Tsuge T, Kanosato M, Doi Y, Abe H. Phase structure and enzymatic degradation of poly(L-lactide)/atactic poly(3-hydroxybutyrate) blends: an atomic force microscopy study. *Biomacromolecules* 2006;7(6):1921-8. doi:10.1021/bm0600163.
- [41] Rydz J, Wolna-Stypka K, Musioł M, Szeluga U, Janeczek H, Kowalczyk M. Further evidence of polylactide degradation in paraffin and in selected protic media. A thermal analysis of eroded polylactide films. *Polym Degrad Stab* 2013;98(8):1450-1457. doi:10.1016/j.polymdegradstab.2013.05.005.
- [42] Rollett AD, De Graef M. Microstructure-Properties Lecture 1: What is Microstructure? [Online], November 2, 2015. http://pajarito.materials.cmu.edu/rollett/27301/L12-Composites-part_2-9Nov15.pptx (accessed November 28, 2017).
- [43] Hossain MR, Islam MA, Vuurea AV, Verpoest I. Effect of fiber orientation on the tensile properties of jute epoxy laminated composite. *J Sci Res* 2013;5(1):43-54. doi:10.3329/jsr.v5i1.10519.
- [44] Ben-Gurion. Chapter 16: Composites. pp. 577-617. [Online], December 31, 2005, <http://in.bgu.ac.il/engn/mater/Documents/LaboratoryBriefings/4/Materials%20Science%20and%20Engineering%20introduction%20Chapter%2015%20Composites%207th%20ed.pdf> (accessed November 30, 2017). doi:10.1007/s10973-016-5311-3.
- [45] Grzabka-Zasadzińska A, Kłapiszewski Ł, Bula K, Jesionowski T, Borysiak S. Supramolecular structure and nucleation ability of polylactide based composites with

silica/lignin hybrid fillers. *J Therm Anal Calorim* 2016;126:263-275. doi:10.1007/s10973-016-5311-3.

[46] Sterzyński T. Processing and property improvement in isotactic polypropylene by heterogeneous nucleation. *Polimery* 2000;45(11-12):786- 791.

[47] Liu X, Wang T, Chow LC, Yang M, Mitchell JW. Effects of inorganic fillers on the thermal and mechanical properties of poly(lactic acid). *Int J Polym Sci* 2014;2014(827028):8 pages. doi:10.1155/2014/827028.

[48] Zhao Y, Keroack D, Prud'homme R. Crystallization under strain and resultant orientation of poly(ϵ -caprolactone) in miscible blends. *Macromolecules* 1999;32:1218-1225. doi:10.1021/ma981416o.

[49] Jamshidian M, Tehrani EA, Imran M, Jacquot M, Desobry S. Poly-lactic acid: production, applications, nanocomposites, and release studies. *Compr Rev Food Sci Food Saf* 2010;9:552-571. doi:10.1111/j.1541-4337.2010.00126.x.

[50] Shaw G, Morse S, Ararat M, Graham FL. Preferential transformation of human neuronal cells by human adenoviruses and the origin of HEK 293 cells. *FASEB J* 2002;6:869-871. doi:10.1096/fj.01-0995fje.

[51] Thomas P, Smart TG. HEK293 cell line: A vehicle for the expression of recombinant proteins. *J Pharmacol Toxicol Methods* 2005;51(3):187-200. doi:10.1016/j.vascn.2004.08.014.

[52] Liang F, Todd BL, Saini RK. Reinforcing amorphous PLA with solid particles for downhole applications. European Patent EP 2764068 A1, September 20, 2012.

[53] Musioł M, Sikorska W, Adamus G, Kowalczyk M. Forensic engineering of advanced polymeric materials. Part III - Biodegradation of thermoformed rigid PLA packaging under

industrial composting conditions. Waste Manage 2016;52:69-76.
doi:10.1016/j.wasman.2016.04.016.

[54] Arrieta MP, Fortunati E, Dominici F, Rayón E, López J, Kenny JM. PLA-PHB/cellulose based films: Mechanical, barrier and disintegration properties. Polym Degrad Stab 2014;107, 139-49. doi:10.1016/j.polymdegradstab.2014.05.010.

[55] Fortunati E, Puglia D, Santulli C, Sarasini F, Kenny JM. Biodegradation of Phormium tenax/poly(lactic acid) composites. J Appl Polym Sci 2012;125:E562-E572. doi:10.1002/app.36839.

[56] Sato H, Murakami R, Mori K, Ando Y, Takahashi O, Noda I, Ozaki Y. Specific crystal structure of poly(3-hydroxybutyrate) thin films studied byinfrared reflection–absorption spectroscopy. Vib Spectrosc 2009;51:132-135. doi:10.1016/j.vibspec.2008.11.010.

[57] Lai SM, Liu YH, Huang CT, Don T-M. Miscibility and toughness improvement of poly(lactic acid)/poly(3-Hydroxybutyrate) blends using a melt-induced degradation approach. J Polym Res 2017;24(102):12 pages. doi:10.1007/s10965-017-1253-0.

[58] Guo Q. Poss-based biodegradable polymers for stent applications: electroprocessing, characterization and controlled drug release, dissertation. Ph.D. Dissertation, Cleveland: Case Western Reserve University, 2010.

Figures captions

Fig. 1. Two different processing build directions: parallel direction (horizontal) and perpendicular direction (vertical) used to obtain the dumbbell-shaped specimens by 3D fused deposition modelling printer.

Fig. 2. ^1H NMR spectrum of PLA/PHA filament.

Fig. 3. ESI-MS spectrum in the range of (A) $m/z = 60-200$ in negative-ion mode and (B) $m/z = 950-1300$ in positive-ion mode of solid sample after 52 weeks of depolymerization in neutral medium at 70 °C of PLA/PHA filament; LA – lactic acid, HB – 3-hydroxybutyrate (86 Da) and HV – 3-hydroxyvalerate (100 Da) constitutional repeating units, AZA – azelaic acid.

Fig. 4. ESI-MS² fragmentation experiment in negative-ion mode for the ion at m/z 187 assigned to azelaic acid (Fig. 3A).

Fig. 5. ESI-MS² fragmentation experiment in positive-ion mode for the ion of the sodium adduct at $m/z = 1259$ belongs to poly(3-hydroxybutyrate-co-3-hydroxyvalerate) (PHBV) series (Fig. 3B).

Fig. 6. Selected SEM micrographs of upper (UH) and underside (BH) layers of PLA dumbbell-shaped specimens surface obtained by 3D printing in horizontal (H) and vertical (V) directions.

Fig. 7. Young's modulus, tensile strength, and elongation at break of PLA and PLA/PHA dumbbell-shaped specimens obtained by 3D printing in horizontal (H) and vertical (V) directions.

Fig. 8. Macro- and micrographic images of the PLA and PLA/PHA dumbbell-shaped specimens obtained by 3D printing in horizontal (H) and vertical (V) directions after tensile test.

Fig. 9. Selected photomicrographs (400x magnification): (A) WI-38 fibroblasts cells with expected irregular morphology, (B) HEK293 cells showing neuron-like shapes.

Fig. 10. Selected SEM micrographs of cells at 500x magnification after 2 days and 7 days incubation on horizontally (H) and vertically (V) printed PLA/PHA blend specimens. Images sequentially illustrate control test (specimen without cells), specimens with WI-38 cells and specimens with HEK293 cells.

Fig. 11. Selected photomicrographs (40x and 400x magnification) of HEK293 cell growth after 2 days and 7 days incubation on horizontally (H) and (V) vertically printed PLA/PHA blend specimens.

Fig. 12. MTT assay of HEK293 cells on horizontally and vertically printed specimens, where absorbencies (at 540 nm) in arbitrary units are equivalent to formazan absorbance as a measure of cell proliferation. The vertical error bars represent standard error based on three replications.

Fig. 13. Macrographic images of the PLA and PLA/PHA dumbbell-shaped specimens obtained by 3D printing in horizontal (H) and vertical (V) directions before and during hydrolytic degradation test at 50 °C and 70 °C.

Fig. 14. Selected SEM micrographs of fractures of PLA and PLA/PHA dumbbell-shaped specimens obtained by 3D printing in horizontal (H) and vertical (V) directions before degradation (0) and at the equal molar mass loss after 70 days of hydrolytic degradation test at 50 °C and after 7 days of hydrolytic degradation test at 70 °C.

Fig. 15. Selected photomicrographs (120x) of underside and upper layers of PLA and PLA/PHA dumbbell-shaped specimens surface obtained by 3D printing in horizontal (H) and vertical (V) directions before and after 42 days under hydrolytic degradation test at 50 °C and 70 °C.

Fig. 16. Overlay of selected FTIR spectra of PLA/PHA dumbbell-shaped specimens obtained by 3D printing in horizontal (H) and vertical (V) directions before (0) and after 7, 21, 42 days of degradation at 50 °C and 70 °C.

Fig. 17. Overlay of selected TG and first-derivative TG thermograms (DTG) of PLA and PLA/PHA dumbbell-shaped specimens obtained by 3D printing in horizontal (solid line on the graph) and vertical (dotted line on the chart) directions before (0) and after 7, 21, 42 days of degradation at 70 °C.

Tables captions

Table 1. Thermal properties of the filaments used.

Table 2. Printer settings for preparation dumbbell-shaped specimens.

Table 3. Calorimetric parameters of PLA and PLA/PHA filament and dumbbell-shaped specimens obtained by 3D printing in horizontal (H) and vertical (V) directions (I-heating run and II-heating run after rapid cooling, 20 °C/min).

- Contact time with printer platform alters the thermal and mechanical properties of materials.
- Filament arrangement from the algorithm used for printing affects material properties.
- Processing conditions lead to different degradation profile of the investigated specimens.
- 3D printed specimens showed good biocompatibility with HEK293 cells.